OPEN ACCESS Freely available online

PLOS | COMPUTATIONAL BIOLOGY

Two Misfolding Routes for the Prion Protein around pH 4.5

Julian Garrec, Ivano Tavernelli, Ursula Rothlisberger*

Laboratory of Computational Chemistry and Biochemistry - Institute of Chemical Sciences and Engineering, École Polytechnique Fédérale de Lausanne, Lausanne, Switzerland

Abstract

Using molecular dynamics simulations, we show that the prion protein (PrP) exhibits a dual behavior, with two possible transition routes, upon protonation of H187 around pH 4.5, which mimics specific conditions encountered in endosomes. Our results suggest a picture in which the protonated imidazole ring of H187 experiences an electrostatic repulsion with the nearby guanidinium group of R136, to which the system responds by pushing either H187 or R136 sidechains away from their native cavities. The regions to which H187 and R136 are linked, namely the C-terminal part of H2 and the loop connecting S1 to H1, respectively, are affected in a different manner depending on which pathway is taken. Specific *in vivo* or *in vitro* conditions, such as the presence of molecular chaperones or a particular experimental setup, may favor one transition pathway over the other, which can result in very different PrP^{Sc} monomers. This has some possible connections with the observation of various fibril morphologies and the outcome of prion strains. In addition, the finding that the interaction of H187 with R136 is a weak point in mammalian PrP is supported by the absence of the {H187,R136} residue pair in non-mammalian species that are known to be resistant to prion diseases.

Citation: Garrec J, Tavernelli I, Rothlisberger U (2013) Two Misfolding Routes for the Prion Protein around pH 4.5. PLoS Comput Biol 9(5): e1003057. doi:10.1371/journal.pcbi.1003057

Editor: Michael Gilson, University of California San Diego, United States of America

Received August 26, 2012; **Accepted** March 27, 2013; **Published** May 16, 2013

Funding: Swiss NSF Grants No. 200020-130082 and 200021-137717 are acknowledged for funding. The funders had no role in study design, data collection and analysis, decision to publish, or preparation of the manuscript.

Competing Interests: The authors have declared that no competing interests exist.

* E-mail: ursula.roethlisberger@epfl.ch

Introduction

The misfolding of the prion protein (PrP), which is a key aspect of transmissible spongiform encephalopathies (TSE), has been the subject of intense research during the past decades. Nonetheless, little is known about the underlying molecular mechanism. One serious hurdle remains the determination of the structure of the resulting misfolded isoform (PrP^{Sc}) [1]. As a consequence, various PrP^{Sc} models have been suggested with substantially different packing arrangements and monomer structures, and a consensus about the structure of PrP^{Sc} is far from being reached [1]. A particular subject of controversy is about the actual region of PrP that undergoes a deep refolding during the PrP $\rightarrow$ PrP^{Sc} conversion. According to the so-called "spiral" [2] and "$\beta-$helix" [3,4] models, extended $\beta-$sheets are formed in the N-terminal region and at the beginning of the C-terminal domain up to H1 (H1 is kept intact in the former and is refolded in the latter model). However, it has been recently shown that the H2H3 core is also highly fibrillogenic by itself [5,6]. Finally, it has also been suggested that PrP^{Sc} could be entirely refolded in an in-register extended $\beta-$sheet [7].

Many in vitro [5,8–11] and computational [2,12–16] studies have tackled this issue using acidic conditions. They have consistently shown that low pH destabilizes PrP and favors its misfolding. This represents biologically relevant conditions insofar as endosomal organelles, whose typical pH is about 5 but can be as low as 4.3 [17], have been highlighted as possible locations for PrP^{Sc} growth [18–20]. Importantly, mammalian PrP contain one slightly buried residue, H187, that titrates right in the range of endosomal pH [11,13]. Several lines of evidence indicate that its protonation [13], or more generally the addition of a positive charge at site 187 [11], destabilizes the protein fold.

Whereas many theoretical studies have been performed on the globular C-terminal domain (residues 121–231 using the numbering of the human sequence) of mouse PrP (mPrP, Fig. 1-A), it is worth noting that the cellular form of PrP (PrP^{C}) also contains a long unstructured N-terminal tail (residues 23–120) [21–29], a glycosylphosphatidyl-inositol (GPI) anchor [30–32] and can be mono or diglycosylated [27,33]. Nevertheless, previous MD simulations have suggested that the structure and dynamics of the globular domain of PrP^{C} is rather independent of the anchoring to the membrane and the glycosylation [34]. In addition, our previous study of the misfolding propensity of mPrP using extensive REMD simulations [16] has revealed that various $\beta-$rich monomers can be formed from the C-terminal domain alone, which is also consistent with the results of Ref. [5,6].

Here, we have performed microsecond MD simulations of the structured C-terminal domain of mPrP at pH 4.5, which corresponds approximately to the lowest pH value observed in endosomes [17]. To this end, we assigned the protonation state of all titrable residues with the program PROPKA [35] (see also Materials and Methods section). The only buried residue for which the protonation state cannot be uniquely assigned is H187. The quantitative evaluation of its pK_a is challenging, because the protonation/deprotonation of a buried residue usually affects the protein structure drastically [36,37]. Nevertheless, several semi-

Author Summary

Transmissible spongiform encephalopathies, which include the "mad cow" disease and the Creutzfeldt-Jakob disease, are related to the abnormal folding of a host protein termed the prion protein (PrP). Many aspects of the underlying molecular mechanism still remain elusive. Among the hypotheses that have been put forward in the past few years, it has been suggested that PrP could be destabilized by the protonation of a specific residue, H187, when the protein passes through acidic cell organelles. We have modeled PrP at the atomistic level, with the neutral and protonated forms of H187. Our simulations show that the destabilization process can follow two alternative pathways that could lead to different final structures. This discovery may shed some light on one of the most puzzling aspect of prion diseases, the fact that they exhibit various strains encoded in the structure of misfolded PrP. In addition, the atomistic details provided by our model highlight a key interactions partner in the destabilization process, R136. The {H187,R136} residue pair is not present in non-mammalian species that do not develop prion diseases.

quantitative estimates of the pK_a of H187 have been obtained [13,38] and they all indicate that mPrP coexists in both, neutral and protonated-H187 forms at pH 4.5. Thus we have performed two sets of acidic pH simulations, with H187 in either its neutral or protonated form. It is worth noting that other residues in mPrP also titrate at pH 4.5. However, they are all located at the protein surface, so that their electrostatic effect on the global structure of the protein is much less important than that of H187. Thus, we have considered only one protonation state for these residues (see Materials and Methods section).

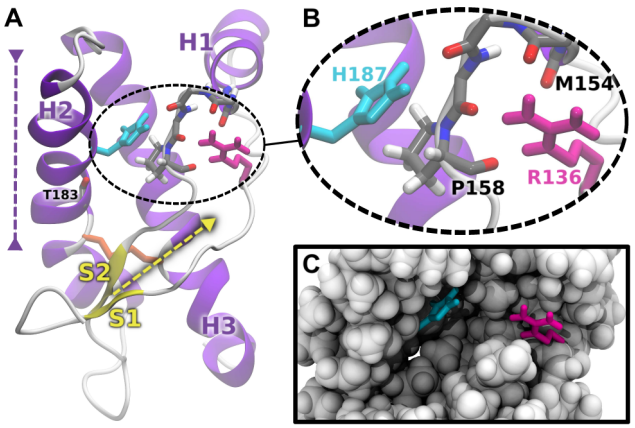

Figure 1. NMR structure of the C-terminal domain of recombinant mouse prion protein (PDB code 1AG2 [21]). (A) Detailed structure showing the secondary structure elements (following the sequence, S1, H1, S2, H2 and H3). The yellow and purple dashed arrows indicate, respectively, the direction of the S1,S2 $\beta-$sheet elongation and the partial unraveling of H2 that we observed in our simulations with a protonated H187 (see text). The disulfide bridge is represented in orange sticks. (B) Zoom on the H187,R136 pair and the $]H1-S2[$ loop (residues 154–158). H187 and R136 are colored in cyan and magenta respectively. Only polar hydrogens and hydrogens of the P158 ring are indicated for clarity. (C) van der Waals surface of the protein arround the solvent-exposed cavities hosting H187 and R136.
doi:10.1371/journal.pcbi.1003057.g001

Our micorsecond simulations show that the mechanism of mPrP destabilization upon protonation of H187 involves R136 as a key partner (Fig. 1-B,C). There is an electrostatic repulsion between the imidazole ring of the protonated H187 ($Im_{H187}H^+$) and the guanidinium group of R136 (Gu^+_{R136}), to which the system responds by pushing away either $Im_{H187}H^+$ or Gu^+_{R136}. Because R136 and H187 belong to two very different structural regions of the protein, namely the loop connecting S1 to H1 ($]S1-H1[$) and the C-terminal part of H2 (H2(Cter), Fig. 1-A), the effect on the structure is different depending on which of the two transition routes is taken. It is possible that specific *in vivo* or *in vitro* conditions may favor one route over the other, which could lead to completely different PrP^{Sc} structures. Our findings thus seems to provide some rational to the various conclusions reached by different authors regarding the actual region of the protein that is refolded upon misfolding.

Results/Discussion

Conformational changes of the backbone

Fig. 2 shows the effect of protonating H187 on the backbone of mPrP. The structure is very stable and remains close to the NMR structure when H187 is neutral, whereas simulations with the protonated H187 exhibit important backbone fluctuations and reorganizations. As depicted in Fig. 2-C, these enhanced fluctuations are mainly located in two specific regions of the protein, namely H2(Cter), which hosts H187, and $]S1-H1[$.

Fig. 2-E shows that the protonation of H187 induces a drastic change in the free energy surface. The projection of the free energy on the $C_\alpha-$RMSDs of H2(Cter) and $]S1-H1[$ shows a single minimum when H187 is neutral, which corresponds to the native structure of PrP, and a complicated multiple minima landscape when H187 is protonated. The new free energy basins are located $\sim 3-6$ Å away from the native basin, thus corresponding to substantial conformational changes.

The two example snapshots provided in Fig. 2-B,D show that this reorganization is accompanied by a significant modification of the secondary structure of the protein. We will provide a more detailed analysis of the secondary structure changes later in the following sections. For the time being, it is interesting to rationalize how the perturbation that is introduced at one side of the protein (the protonation of H187 located in H2(Cter)) is transmitted through the macromolecule and affects strongly the structure at the opposite side ($]S1-H1[$).

Reorganization of charged residues around H187

In order to understand the mechanism by which the protonation of H187 induces the reorganization of the protein structure, it is necessary to have a closer look to the environment of H187 in PrP. It is particularly interesting to focus on nearby charged residues because they are expected to play a major role in the reorganization of the protein when H187 gets a positive charge upon protonation. In the NMR structure of mouse PrP, the closest charged residues are R136, R156, K194, E196 and D202 (Fig. S5-A). R136 is somewhat isolated in terms of proximity with charged residues other than H187 (when protonated), whereas K194, E196, R156, and D202 form a network of salt-bridge interactions. These four latter residues have been pointed out has possible key residues in the misfolding of PrP [13,39]. As shown in Fig. S5-B, our simulation provide a consistent picture with that of Ref. [13], because the protonation of H187 leads to the disruption of the salt bridge between E196 and R156 and the transient formation of a

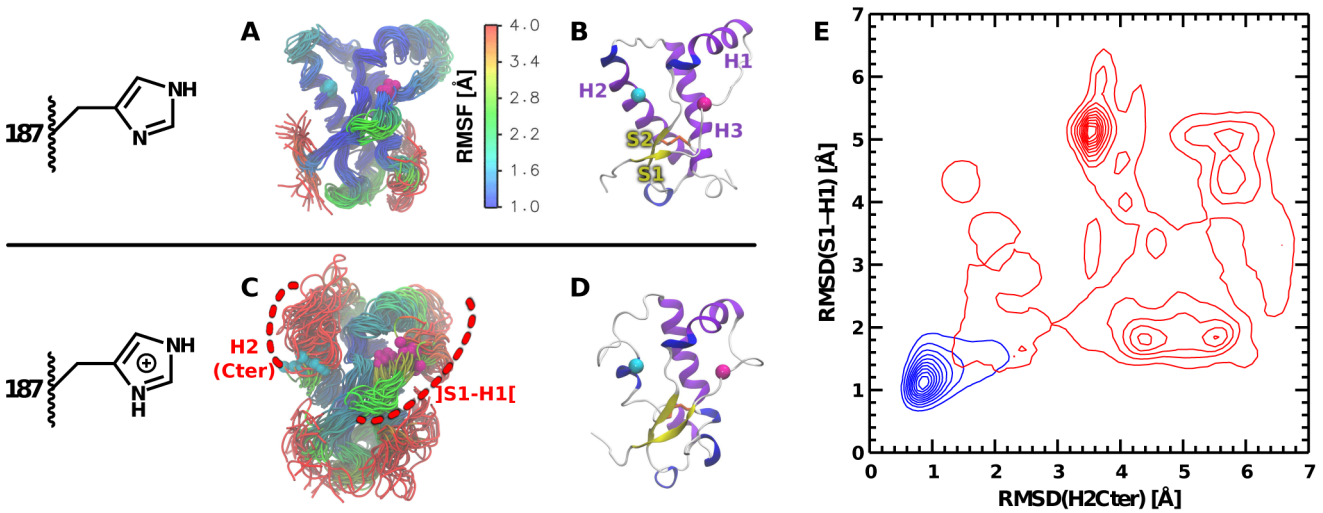

Figure 2. Effect of protonating H187 on the backbone conformation. (A,B) and (C,D) Simulation frames extracted every 50 ns from simulations with a neutral and protonated H187, respectively. The C_α atoms of H187 and R136 are represented with cyan and magenta spheres, respectively. The two regions of high fluctuations when H187 in protonated, H2(Cter) and $]S1-H1[$, are represented by dashed red arcs in panel C. In panels A,C frames were extracted from two independent simulations of 1 μs with a neutral H187 and two independent simulations of 1 μs with a protonated H187, respectively, and colored according to the $C_\alpha-$RMSF. Note that this corresponds to a subset of all our simulation, aimed at providing comparable data between panels A and C. We provide the same representations for each individual simulation in Figure S2. (E) Bivariate distribution of the $C_\alpha-$RMSD in H2(Cter) and $]S1-H1[$. The contour plots are constructed from all the simulations with a neutral (blue) or protonated (red) H187. The reference structure used to compute the RMSD is the average structure calculated from all our simulations with a neutral H187.
doi:10.1371/journal.pcbi.1003057.g002

new salt bridge between the protonated E196 and H187, while a tight salt bridge is maintained between R156 and D202 (K194 is highly solvated, independently of the protonation state of H187, and never interact strongly with E196). Nevertheless, the fact that R136 does not have any close alternative partner makes it more sensitive to the positive electric field created by the protonated H187, as we shall see in the next section.

Dual response of PrP, $187_{in}/136_{out}$ vs $187_{out}/136_{in}$

The observation of structural rearrangements in $]S1-H1[$, which is located far from H187, has motivated us to perform a thorough analysis of the mobility of each residue in this region. It turns out that R136 is a key partner of H187 in the destabilization of mammalian PrP upon protonation of H187. In the NMR structure of mPrP (Fig. 1), Im_{H187} and Gu^+_{R136} are about 8 Å apart and loop $]H1-S2[$ (residues 154–158) is located in between. Gu^+_{R136} is stabilized by a series of dipole-charge interactions with four peptide bonds while Im_{H187} is H-bonded to one carbonyl group and establishes van der Waals contacts with the ring of P158 (Fig. 1-B).

Because of the proximity of Im_{H187} and Gu^+_{R136} in the native structure of mPrP, the protonation of the former should induce an electrostatic repulsion between the two groups. A discussion of the corresponding energetics is provided in Text S1. Fig. 3 shows the effect of the protonation of H187 on the position of Im_{H187} (or $Im_{H187}H^+$) and Gu^+_{R136}. When H187 is neutral, Im_{H187} and Gu^+_{R136} are mostly located in their respective native cavities, whereas they cover a much wider portion of conformational space upon protonation of H187. We define four conformational states according to the position of Im_{H187} (or $Im_{H187}H^+$) and Gu^+_{R136} inside or outside their respective native cavities. To do so we consider the bivariate histogram of the distances between Im_{H187} (or $Im_{H187}H^+$) and Gu^+_{R136} from their respective cavities (Fig. 3-C). The conformational state in which both groups stay close to their original location will be termed $187_{in}/136_{in}$, and we define states $187_{in}/136_{out}$ and $187_{out}/136_{in}$ according to the departure of $Im_{H187}H^+$ or Gu^+_{R136}, respectively. Interestingly, the $187_{out}/136_{out}$ state is almost not populated. The picture that is the most consistent with these data is that PrP exhibits a dual response to the protonation of H187, by pushing away either $Im_{H187}H^+$ or Gu^+_{R136} (but not both at the same time), thus decreasing the electrostatic repulsion between them. Because H187 and R136 are attached to H2(Cter) and $]S1-H1[$, respectively (Fig. 1-A,B), the local reorganization of either $Im_{H187}H^+$ or Gu^+_{R136} affects the global structure of these two regions (Fig. 2). We stress that, once H187 is protonated, the dynamics of the system proceeds smoothly through a series of locally thermalized states giving rise, in a reproducible way, to either the $187_{in}/136_{out}$ or $187_{out}/136_{in}$ state. Fig. S6 and S7 show that $Im_{H187}H^+$ and Gu^+_{R136} remain in their native pockets during at least 100 ns before one of the two moves out.

A similar electrostatic repulsion can be expected for the H187R mutation, for which the positive charge of the introduced arginine has been suggested to destabilize the overall fold of human PrP [11,40,41]. An interesting aspect of this finding is that none of the non-mammalian PrP exhibit this specific $H2(Cter)-Im_{H187}H^+\cdots]H1-S2[\cdots Gu^+_{R136}-]S1-H1[$ spatial arrangement (Fig. S4). In other words, these non-mammalian proteins do not have this pH-sensitive "weak point" in there structure and this probably explains the fact that non-mammalian species do not exhibit TSEs.

Due to the buried character of H187 and the fact that its protonation induces a substantial modification of the protein structure, the quantitative evaluation of its pK_a (and the corresponding contributions of other residues) during the misfolding is challenging [36,37]. Nevertheless, PROPKA calculations [35] provide physically sound estimates that can help to rationalize the underlying physics. Such calculations for representative

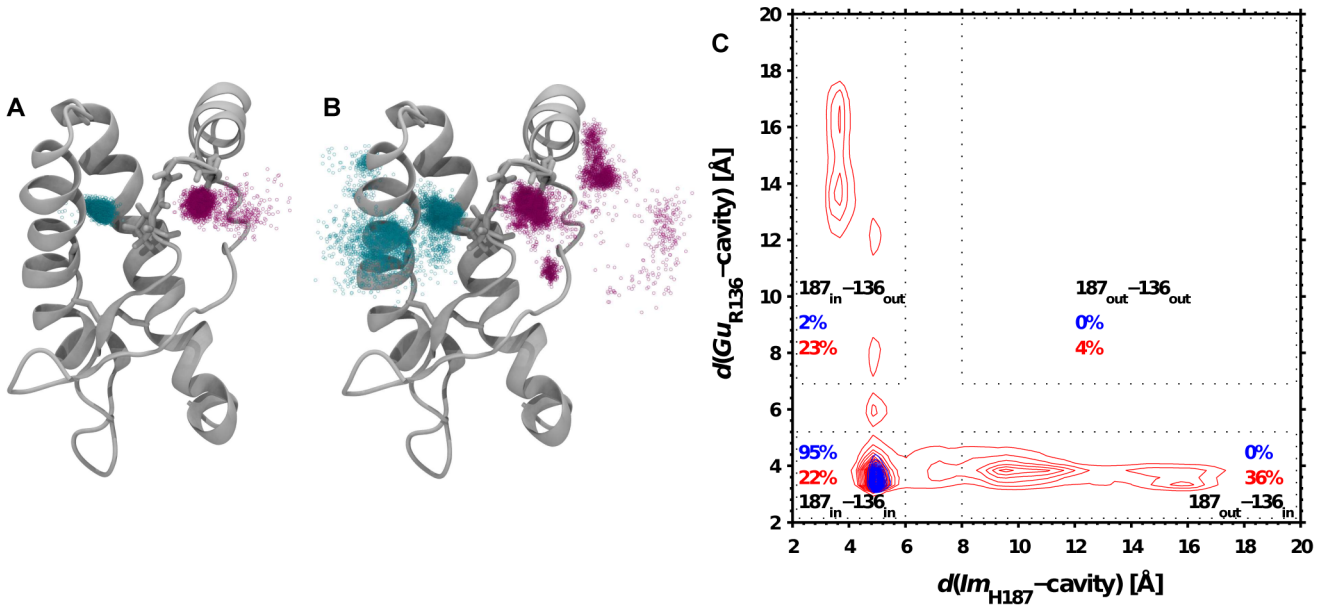

Figure 3. Effect of protonating H187 on the position of Im_{H187} (or $Im_{H187}H^+$) and Gu^+_{R136}. (A) Positions of the H187(C_γ) and R136(C_ζ) atoms in cyan and magenta, respectively. The positions were extracted every 400 ps from two independent simulations of 1 μs with a neutral H187. Note that this figure is aimed at showing general trends and only represents a subset of all our simulations. We provide the same representations for each individual simulation in Figure S3. (B) Same as (A) but with a protonated H187. (C) Bivariate distribution of the distances between Im_{H187} (or $Im_{H187}H^+$) or Gu^+_{R136} and their respective cavities ($P[d(Im_{H187}-\text{cavity}), d(Gu^+_{R136}-\text{cavity})]$). The contour plots are constructed from all the simulations with a neutral (blue) or protonated (red) H187. $d(Im_{H187}-\text{cavity})$ and $d(Gu^+_{R136}-\text{cavity})$ are defined as the distance between the H187(C_γ) atom and the R156(O) atom and the distance between the R136(C_ζ) atom and the Y157(O) atom, respectively. The conformational basins ($187_{in}/136_{in}$, $187_{in}/136_{out}$ and $187_{out}/136_{in}$, see text) are defined according to the cutoff distances represented by dotted rectangles. The regions with intermediate value are excluded.
doi:10.1371/journal.pcbi.1003057.g003

snapshots of our simulations are provided in Fig. S8. The pK_a of H187 is systematically shifted up as soon as the protein starts to misfold, independently of the pathway ($187_{in}/136_{out}$ vs $187_{out}/136_{in}$) that is taken. This is in agreement with the fact that the proximity with the positive charge of Gu^+_{R136} in the native structure of mPrP induces a down-shift of the pK_a of H187 (this is supported by the fact that our PROPKA calculations report R136 as a key residue in the electrostatic environment of H187, see the corresponding PROPKA output file for a representative $187_{in}/136_{in}$ structure in Dataset S1). As soon as Gu^+_{R136} moves out of its cavity ($187_{in}/136_{out}$ state) the electrostatic repulsion between $Im_{H187}H^+$ and Gu^+_{R136} decreases and the protonated form of H187 becomes much more stable (pK_a shifted up). When the protein adopts a $187_{out}/136_{in}$ state, $Im_{H187}H^+$ is much more solvated by water and the pK_a of H187 approaches the corresponding value in water ($\sim$6).

S1,S2 elongation

The positioning of Im_{H187} (or $Im_{H187}H^+$) and Gu^+_{R136} has a strong influence on the length of the S1,S2 $\beta-$sheet, as shown in Table 1. Typically, both $187_{in}/136_{in}$ and $187_{out}/136_{in}$ states correspond to structures with a short native $\beta-$sheet, while the $187_{in}/136_{out}$ state is characterized by the preference of an elongated $\beta-$sheet. This is illustrated by the simulation depicted in Fig. 4. At the beginning of the simulation, the protein is in its native conformation. As depicted in the insets of Fig. 4, the native location of Gu^+_{R136} at $t\sim0$ is a key aspect of the protein fold because it forms a sort of "clip" that forces the $]S1-H1[$ backbone to remain packed against the rest of the protein (Fig. 1-A) in a specific conformation. The permanent departure of Gu^+_{R136} out of its cavity at $t\approx350$ ns induces an important release of $]S1-H1[$ backbone constraint and the system is consequently more prone to reorganize in this region. Then the system relaxes during about 400 ns, and $]S1-H1[$ and $]H1-S2[$ come close together. The number of hydrogen bonds between the two strands increases concomitantly and the $\beta-$sheet elongates (Fig. 4-A,B).

H2 unraveling

As shown in Fig. 5, both $187_{out}/136_{in}$ and $187_{in}/136_{out}$ states are characterized by an unraveling of H2(Cter). However, the underlying mechanisms (and the corresponding transition pathways) differ substantially. The portion of the helix that undergoes an unraveling is represented by a dashed purple arrow in Fig. 1-A (see also the example snapshot depicted in Fig. 2-D).

The departure of $Im_{H187}H^+$ ($187_{out}/136_{in}$ conformation) out of its cavity obviously destabilizes H2 because the helix looses a key tertiary contact with loop $]H1-S2[$ (Fig. 1-A). The unraveling of H2(Cter) in the $187_{in}/136_{out}$ state has its roots in the polar interactions of $Im_{H187}H^+$ with the nearby residues. A closer look to the shape of the Im_{H187} cavity (Fig. 1) reveals that it is a narrow groove at the bottom of which lies the carbonyl group of T183. The contact analysis shown in Fig. 6 reveals that the neutral Im_{H187} is H-bonded to R156 only, consistent with the NMR structure of mPrP [21], whereas new contacts are formed with the CO group of T183 when H187 is protonated. A key aspect of these extra contacts is that they involve not only the $N_{\delta1}-H$ group of H187, but also the $C_{\delta2}-H$ group. They reflect dipole-charge interactions between the extra positive charge of $Im_{H187}H^+$ and the dipole moments of the 156–157 and 182–183 peptide bonds. In other words, the imidazole ring can take two conformations around the $C_\beta-C\gamma$ bond and still maintain a

Table 1. Number of short/long $\beta-$sheets.

	$187_{in}/136_{in}$ [b]	$187_{in}/136_{out}$ [c]	$187_{out}/136_{in}$ [c]
Population of short $\beta-$sheets [%] [a]	93.2	65.3	99.0
Population of long $\beta-$sheets [%] [a]	6.8	34.7	1.0

[a]The number of residues in a β conformation in the structures of mammalian PrP taken in the PDB is either 4 or 6. Hence we define a short and a long $\beta-$sheet as a $\beta-$sheet with a number of residues ≤ 6 or >6, respectively. The populations are in % of the corresponding cluster.
[b]Cluster extracted from the simulations with a neutral H187.
[c]Cluster extracted from the simulations with a protonated H187.
doi:10.1371/journal.pcbi.1003057.t001

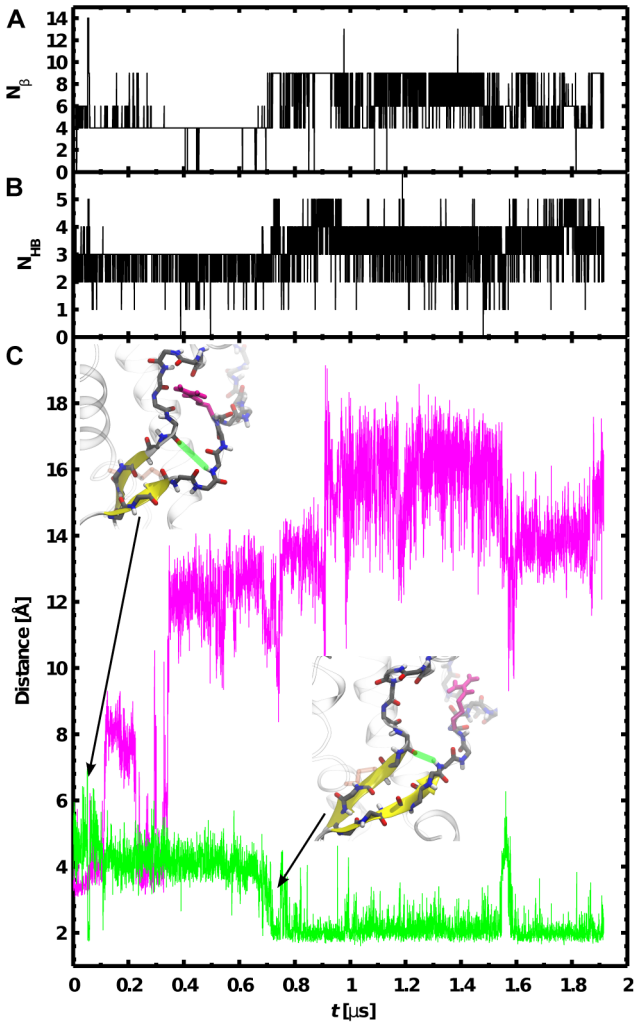

Figure 4. Link between the motion of Gu^+_{R136} toward bulk water and the elongation of S1,S2. The data are taken from a simulation in which a $187_{in}/136_{out}$ state is formed permanently. (A) Time evolution of the number of residues in a β conformation. (B) Time evolution of the number of backbone hydrogen bond between $]S1-H1[$ and $]H1-S2[$ (the backbone atoms of these two loops are represented with sticks in the two MD snapshots shown in panel C). (C) Time series of $d(Gu^+_{R136}-\text{cavity})$ (same definition as in Fig. 3) and the distance between the extremities of the two strands (represented with a thick green line in the two MD snapshots).
doi:10.1371/journal.pcbi.1003057.g004

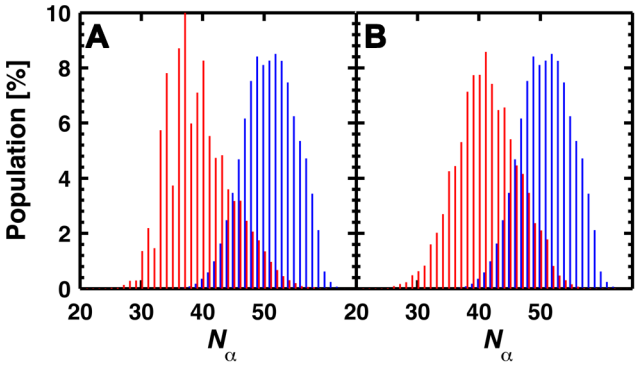

Figure 5. Effect of the $187_{in}/136_{out}$ and $187_{out}/136_{in}$ conformations on the number of helical residues (N_α). (A) Distribution of N_α in the $187_{in}/136_{out}$ cluster extracted from simulations with a protonated H187 (red) compared to the $187_{in}/136_{in}$ cluster extracted from simulations with a neutral H187 (blue). (B) Distribution of N_α in the $187_{out}/136_{in}$ state extracted from simulations with a protonated H187 (red) compared to the $187_{in}/136_{in}$ state extracted from simulations with a neutral H187 (blue). The populations are in % of the corresponding cluster.
doi:10.1371/journal.pcbi.1003057.g005

significant interaction with one of the two nearby backbone CO groups, which results in four stable conformations inside the pocket.

The formation of new contacts between $Im_{H187}H^+$ and T183(CO) has two effects that explain the loss of helical character in H2(Cter). First of all, it weakens the tertiary contact between H2(Cter) and $]H1-S2[$. Second, the native intra-helix H-bond between T183(CO) and H187(NH) is lost. The tighter the interaction between $Im_{H187}H^+$ and T183(CO) the weaker the local stability of H2.

Concluding remarks

In this paper we have shown that the protonation of H187 in mPrP at pH 4.5, which corresponds approximately to the lowest pH observed in endosomes [17], leads to extensive conformational changes on the microsecond time scale. The picture that emerges

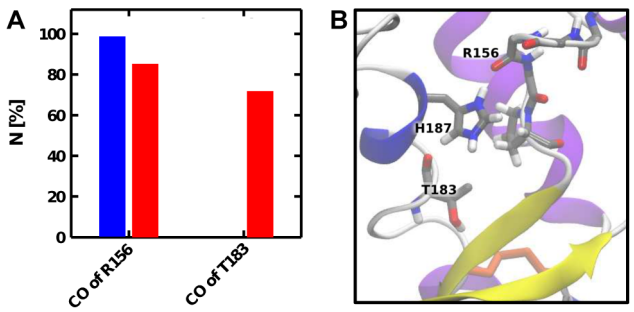

Figure 6. Polar interactions of $Im_{H187}H^+$ in its cavity when the system is in the $187_{in}/136_{out}$ state. (A) Number of contacts (N) between Im_{H187} (or $Im_{H187}H^+$) and the CO groups of R156 and T183 in the $187_{in}/136_{out}$ cluster extracted from simulations with a protonated H187 (red) compared to the $187_{in}/136_{in}$ cluster extracted from simulations with a neutral H187 (blue). (B) Example snapshot showing $Im_{H187}H^+$ interacting with both CO groups when the systems is in the $187_{in}/136_{out}$ state. Note that $Im_{H187}H^+$ can interact with R156(CO) alone, T183(CO) alone, or both.
doi:10.1371/journal.pcbi.1003057.g006

from our simulations is that the protonation of H187 leads to an electrostatic repulsion between the positive charges of $Im_{H187}H^+$ and Gu^+_{R136}, which results in conformational transitions in the regions to which H187 and R136 are linked, namely H2(Cter) and $]S1-H1[$ respectively.

Our findings hence highlight two possible routes for PrP misfolding with either the unraveling of H2(Cter) alone ($187_{out}/136_{in}$ route) or the unraveling of H2(Cter) with simultaneous elongation of S1,S2 ($187_{in}/136_{out}$ route). This dual behavior seems to reconcile the various observations and proposals that have been made regarding the actual PrP region that undergoes a deep refolding upon conversion to PrP^{Sc} [2–5]. It is indeed possible that a particular computational or experimental setup favors one of the $187_{in}/136_{out}$ or $187_{out}/136_{in}$ substates at the beginning of the misfolding process. Such conformational shift could be assisted *in vivo* by molecular chaperones such as polyanionic molecules [1,42]. This variability in misfolding pathways may also be connected to the fact that prion exhibits a variety of strains, because it is believed that changes in conformations of PrP^{Sc} encodes for strain properties [30,43,44].

Finally, it is interesting to note that the $H2(Cter)-Im_{H187}H^+\cdots]H1-S2[\cdots Gu^+_{R136}-]S1-H1[$ pattern is not present in those non-mammalian species who are known to resist to TSEs. This is a possible explanation for the observed resistance to TSEs in these species.

Materials and Methods

Initial structure and protonation state

All simulations were started from the NMR structure of mPrP published by Riek *et al.* (PDB code 1AG2). We aimed at modeling mPrP with a neutral or protonated H187 at pH 4.5.

The protonation state of titrable residues apart from H187 was first estimated from PROPKA [35] calculations. The protonation state of most of them can be determined without ambiguity. All buried or semi-buried residues other than H187 are all aspartic or glutamic acids whose side chains are hydrogen-bonded to other groups in the protein. This has the effect to shift up their pK_a above the typical values of ~ 4 that they adopt in water, i.e. significantly above the pH we want to model. Hence they are expected to be protonated. The solvent-exposed histidines are expected to exhibit a pK_a of ~ 6 so they can be considered protonated at a pH of 4.5. The remaining solvent-exposed aspartic or glutamic acids are more ambiguous because their pK_a is close to the pH we want to model. Nevertheless, their solvent-exposed character makes them much less important for the global fold of the protein. We chose their protonation state according to the pK_a estimated with PROPKA [35]. The relevance of this choice was verified *a posteriori* by observing that the fold of the protein is very well conserved over microsecond simulations with a neutral H187.

Simulation setup

Two topologies (one with H187 neutral and one with H187 protonated) were built with the GROMACS 4.0.7 [45–47] suite of programs. For each of them, the protein was immersed in a rhombic dodecahedral water box. The size of the box was chosen so that the distance between the protein and the edge of the box was ≈ 15 Å. The system was neutralized by adding 2 or 3 chloride counterions (depending on the protonation state of H187). The resulting system contained about 30000 atoms.

The AMBER99SB force field [48] was used to describe the protein and the TIP3P model [49] was employed for the water molecules. The force field was included in GROMACS thanks to the ports provided by Sorin and coworkers [50,51]. The particle mesh Ewald method [52] together with a Fourier grid spacing of 1 Å and a cutoff of 12 Å was used to treat long-range electrostatic interactions. A cutoff of 12 Å was used for van der Waals interactions. The water box was first relaxed by means of NpT simulations with restraints applied to the positions of the heavy atoms of the protein. Then the system was optimized in a series of energy minimization runs in which the restraints on the protein were progressively removed. Finally, we run eight simulations with a time step of 2 fs. Three and five of them were conducted with a neutral or protonated H187, respectively.

Each simulation was initiated with a set of velocities taken at random from a Maxwell-Boltzmann distribution corresponding to a temperature of 10 K. Then the system was heated up to 300 K in 300 ps using two Berendsen thermostats [53] (one for the protein and one for the solvent) with a relaxation time of 0.1 ps each. The simulation was prolonged for 100 ps and the Berendsen barostat with a relaxation time of 2 ps was switched on during 100 ps. Finally, we switched to production phase using a Nose-Hoover [54,55] thermostat and a Parrinello-Rahman barostat [56] with relaxation times of 0.5 and 10.0 ps, respectively. The total simulation lengths were 1.9, 1.3 and 1.6 μs for simulations with a neutral H187, and 1.9, 1.5, 1.6, 1.2 and 1.2 μs for simulations with a protonated H187. The $C_\alpha-RMSD$ plot of each simulation is provided in Figure S1.

Molecular visualization and analysis

All the representations were done with the program VMD [57]. Secondary structure assignments were done using the STRIDE algorithm [58].

Supporting Information

Text S1 Energetics of the $Im_{H187}H^+$ - Gu^+_{R136} ion pair in the native structure of mPrP. Estimation of the electrostatic interaction between $Im_{H187}H^+$ and Gu^+_{R136} using a Coulomb-type expression [59–61] and the typical dielectric constant inside a protein [59,61,62]. Discussion of the strength of this interaction and its implication on the protein stability.
(PDF)

Dataset S1 PROPKA [35] output file obtained from a representative structure of a $187_{in}/136_{in}$ state (same structure as Fig. S8-A.).
(TXT)

Dataset S2 PROPKA [35] output file obtained from a representative structure of a $187_{out}/136_{in}$ state (same structure as Fig. S8-B.).
(TXT)

Dataset S3 PROPKA [35] output file obtained from a representative structure of a $187_{in}/136_{out}$ state (same structure as Fig. S8-C.).
(TXT)

Figure S1 $C_\alpha-RMSD$. Each panel corresponds to one individual simulation, differing by the initial velocities extracted at random from a Maxwell-Boltzmann distribution. (A–C) Three individual simulations in which H187 is neutral. (D–H) Five individual simulations in which H187 is protonated.
(TIF)

Figure S2 Backbone fluctuations. Each panel corresponds to one individual simulation, differing by the initial velocities extracted at random from a Maxwell-Boltzmann distribution. (A–C) Three individual simulations in which H187 is neutral. (D–H)

Five individual simulations in which H187 is protonated. Simulation frames are extracted every 50 ns. The C_α atoms of H187 and R136 are represented with cyan and magenta spheres, respectively. The backbone is colored according to the $C_\alpha - \mathrm{RMSF}$ (same scale as Fig. 2).
(TIF)

Figure S3 Position of Im_{H187} (or $Im_{H187}H^+$) and Gu^+_{R136}. The positions of the H187(C_γ) and R136(C_ζ) atoms are represented by cyan and magenta spheres, respectively. Each panel corresponds to one individual simulation, differing by the initial velocities extracted at random from a Maxwell-Boltzmann distribution. (A–C) Three individual simulations in which H187 is neutral. (D–H) Five individual simulations in which H187 is protonated. Simulation frames are extracted every 400 ps.
(TIF)

Figure S4 Mammalian VS non-mammalian species. The upper panel of the figure shows the sequence alignment in the H2(Cter) region. H187 is represented in cyan in the sequence and is conserved throughout all mammalian PrP. The lower panel represents the charged residues in examples of mammalian (mouse) and non-mammalian (chicken) PrP. The geometric center of positively and negatively charged groups are represented by blue and red opaque spheres, respectively. The two transparent spheres in cyan and magenta correspond to the position of Im_{H187} and Gu^+_{R136} in mPrP, respectively. Sequence and structural alignments were done with the MultiSeq plugin [63] implemented in VMD [57].
(TIF)

Figure S5 Charged residues around Im_{H187}. (A) Relative positioning of the residues. All charged groups around Im_{H187} fall approximately within the same range of distance, which is represented by a transparent sphere of 8 Å diameter centered on the geometric center of $Im_{H187}H^+$. (B) Population of salt bridges in our simulations with a neutral (blue) or protonated (red) H187.
(TIF)

Figure S6 Distance of Im_{H187} (or $Im_{H187}H^+$) from its cavity as a function of time. (A–C) Three individual simulations in which H187 is neutral. (D–H) Five individual simulations in which H187 is protonated. The distance $d(\mathrm{Im}_{H187} - \mathrm{cavity})$ is defined as in Fig. 3-C. The magenta box represents the cutoffs used in Fig. 3-C to define $187_{in}/136_{in}$, $187_{in}/136_{out}$, $187_{out}/136_{in}$ and $187_{out}/136_{out}$ states.
(TIF)

Figure S7 Distance of Gu^+_{R136} from its cavity as a function of time. (A–C) Three individual simulations in which H187 is neutral. (D–H) Five individual simulations in which H187 is protonated. The distance $d\left(\mathrm{Gu}^+_{R136} - \mathrm{cavity}\right)$ is defined as in Fig. 3-C. The magenta box represents the cutoffs used in Fig. 3-C to define $187_{in}/136_{in}$, $187_{in}/136_{out}$, $187_{out}/136_{in}$ and $187_{out}/136_{out}$ states.
(TIF)

Figure S8 pK_a of H187 as a function of the relative positioning of $Im_{H187}H^+$ and Gu^+_{R136}. Representative snapshots of (A) a $187_{in}/136_{in}$ state (equilibrated structure before $Im_{H187}H^+$ or Gu^+_{R136} moves out of its cavity), (B) a $187_{out}/136_{in}$ state, and (C) a $187_{in}/136_{out}$ state. Water molecules that are within 3 Å of $Im_{H187}H^+$ or Gu^+_{R136} are represented in cyan and magenta, respectively. The number close to H187 in each panel indicates the pK_a of this residue, as estimated by PROPKA [35] from the corresponding structure. The calculations were performed using the PDB2PQR software [64,65]. We also provide the PROPKA output files corresponding to panels (A), (B) and (C) in Dataset S1, S2 and S3, respectively.
(TIF)

Acknowledgments

The authors thank the DIT/EPFL for the computer time.

Author Contributions

Conceived and designed the experiments: JG IT UR. Performed the experiments: JG. Analyzed the data: JG. Contributed reagents/materials/analysis tools: JG. Wrote the paper: JG.

References

1. Diaz-Espinoza R, Soto C (2012) High-resolution structure of infectious prion protein: the final frontier. Nat Struct Mol Biol 19: 370–377.
2. DeMarco M, Daggett V (2004) From conversion to aggregation: Protobril formation of the prion protein. Proc Natl Acad Sci USA 101: 2293–2298.
3. Govaerts C, Wille H, Prusiner S, Cohen F (2004) Evidence for assembly of prions with left-handed beta-helices into trimers. Proc Natl Acad Sci U S A 101: 8342–8347.
4. Wille H, Bian W, McDonald M, Kendall A, Colby DW, et al. (2009) Natural and synthetic prion structure from x-ray fiber difraction. Proc Natl Acad Sci USA 106: 16990–16995.
5. Adrover M, Pauwels K, Prigent S, de Chiara C, Xu Z, et al. (2010) Prion fibrillization is mediated by a native structural element that comprises helices H2 and H3. J Biol Chem 285: 21004–21012.
6. Xu Z, Prigent S, Deslys JP, Rezaei H (2011) Dual conformation of H2H3 domain of prion protein in mammalian cells. J Biol Chem 286: 40060–40068.
7. Smirnovas V, Baron GS, Offerdahl DK, Raymond GJ, Caughey B, et al. (2011) Structural organization of brain-derived mammalian prions examined by hydrogen-deuterium exchange. Nat Struct Mol Biol 18: 504–506.
8. Swietnicki W, Petersen R, Gambetti P, Surewicz W (1997) pH-dependent stability and conformation of the recombinant human prion protein PrP(90–231). J Biol Chem Chemistry 272: 27517–27520.
9. Hornemann S, Glockshuber R (1998) A scrapie-like unfolding intermediate of the prion protein domain PrP(121–231) induced by acidic pH. Proc Natl Acad Sci U S A 95: 6010–6014.
10. Gerber R, Tahiri-Alaoui A, Hore PJ, James W (2008) Conformational pH dependence of intermediate states during oligomerization of the human prion protein. Protein Sci 17: 537–544.
11. Hosszu LLP, Tattum MH, Jones S, Trevitt CR, Wells MA, et al. (2010) The H187R mutation of the human prion protein induces conversion of recombinant prion protein to the PrP^{Sc}-like form. Biochemistry 49: 8729–8738.
12. Alonso D, DeArmond S, Cohen F, Daggett V (2001) Mapping the early steps in the pH-induced conformational conversion of the prion protein. Proc Natl Acad Sci U S A 98: 2985–2989.
13. Langella E, Improta R, Crescenzi O, Barone V (2006) Assessing the acid-base and conformational properties of histidine residues in human prion protein (125–228) by means of pK_a calculations and molecular dynamics simulations. Proteins Struct Funct Bioinf 64: 167–177.
14. Campos SRR, Machuqueiro M, Baptista AM (2010) Constant-pH molecular dynamics simulations reveal a beta-rich form of the human prion protein. J Phys Chem B 114: 12692–12700.
15. van der Kamp MW, Daggett V (2010) Influence of pH on the human prion protein: Insights into the early steps of misfolding. Biophys J 99: 2289–2298.
16. Baillod P, Garrec J, Colombo MC, Tavernelli I, Rothlisberger U (2012) Enhanced sampling molecular dynamics identifies PrPSc structures harboring a C-terminal beta-core. Biochemistry 51: 9891–9899.
17. Lee R, Wang S, Low P (1996) Measurement of endosome pH following folate receptor-mediated endocytosis. Biochim Biophys Acta 1312: 237–242.
18. Caughey B, Raymond G, Ernst D, Race R (1991) N-terminal truncation of the scrapie-associated form of PrP by lysosomal protease(s): implications regarding the site of conversion of PrP to the protease-resistant state. J Virol 65: 6597–6603.
19. Borchelt D, Taraboulos A, Prusiner S (1992) Evidence for synthesis of scrapie prion proteins in the endocytic pathway. J Biol Chem 267: 16188–16199.
20. Arnold J, Tipler C, Laszlo L, Hope J, Landon M, et al. (1995) The abnormal isoform of the prion protein accumulates in late-endosome-like organelles in scrapie-infected mouse brain. J Pathol 176: 403–411.
21. Riek R, Hornemann S, Wider G, Billeter M, Glockshuber R, et al. (1996) NMR structure of the mouse prion protein domain PrP(121–231). Nature 382: 180–182.
22. Donne D, Viles J, Groth D, Mehlhorn I, James T, et al. (1997) Structure of the recombinant full-length hamster prion protein prp(29–231): The n terminus is

highly exible. Proceedings of the National Academy of Sciences of the United States of America 94: 13452–13457.
23. Riek R, Hornemann S, Wider G, Glockshuber R, Wuthrich K (1997) Nmr characterization of the full-length recombinant murine prion protein, mprp(23–231). Febs Letters 413: 282–288.
24. Hornemann S, Korth C, Oesch B, Riek R, Wider G, et al. (1997) Recombinant full-length murine prion protein, mprp(23–231): purification and spectroscopic characterization. Febs Letters 413: 277–281.
25. Zahn R, Liu A, Luhrs T, Riek R, von Schroetter C, et al. (2000) Nmr solution structure of the human prion protein. Proceedings of the National Academy of Sciences of the United States of America 97: 145–150.
26. Garcia F, Zahn R, Riek R, Wuthrich K (2000) Nmr structure of the bovine prion protein. Proceedings of the National Academy of Sciences of the United States of America 97: 8334–8339.
27. Wuthrich K, Riek R (2001) Three-dimensional structures of prion proteins. Advances In Protein Chemistry 57: 55–82.
28. Knaus K, Morillas M, Swietnicki W, Malone M, Surewicz W, et al. (2001) Crystal structure of the human prion protein reveals a mechanism for oligomerization. Nature Structural Biology 8: 770–774.
29. Calzolai L, Lysek D, Perez D, Guntert P, Wuthrich K (2005) Prion protein nmr structures of chickens, turtles, and frogs. Proc Natl Acad Sci USA 102: 651–655.
30. Prusiner SB (1998) Prions. Proc Natl Acad Sci U S A 95: 13363–13383.
31. Collinge J (2001) Prion diseases of humans and animals: Their causes and molecular basis. Annual Review of Neuroscience 24: 519–550.
32. Aguzzi A, Calella AM (2009) Prions: Protein aggregation and infectious diseases. Physiological Reviews 89: 1105–1152.
33. Haraguchi T, Fisher S, Olofsson S, Endo T, Groth D, et al. (1989) Asparagine-linked glycosylation of the scrapie and cellular prion proteins. Archives of Biochemistry and Biophysics 274: 1–13.
34. DeMarco M, Daggett V (2009) Characterization of cell-surface prion protein relative to its recombinant analogue: insights from molecular dynamics simulations of diglycosylated, membrane-bound human prion protein. J Neurochem 109: 60–73.
35. Li H, Robertson A, Jensen J (2005) Very fast empirical prediction and rationalization of protein pK_a values. Proteins Struct Funct Bioinf 61: 704–721.
36. Warshel A (1981) Calculations of enzymatic-reactions - Calculations of pka, proton-transfer reactions, and general acid catalysis reactions in enzymes. Biochemistry 20: 3167–3177.
37. Kato M, Warshel A (2006) Using a charging coordinate in studies of ionization induced partial unfolding. J Phys Chem B 110: 11566–11570.
38. Langella E, Improta R, Barone V (2004) Checking the pH-induced conformational transition of prion protein by molecular dynamics simulations: Effect of protonation of histidine residues. Biophys J 87: 3623–3632.
39. Calzolai L, Zahn R (2003) Inuence of pH on NMR structure and stability of the human prion protein globular domain. J Biol Chem 278: 35592–35596.
40. Zhong L (2010) Exposure of hydrophobic core in human prion protein pathogenic mutant h187r. Journal of Biomolecular Structure & Dynamics 28: 355–361.
41. Rossetti G, Cong X, Caliandro R, Legname G, Carloni P (2011) Common structural traits across pathogenic mutants of the human prion protein and their implications for familial prion diseases. Journal of Molecular Biology 411: 700–712.
42. Caughey B, Baron GS (2006) Prions and their partners in crime. Nature 443: 803–810.
43. Castilla J, Morales R, Saa P, Barria M, Gambetti P, et al. (2008) Cell-free propagation of prion strains. EMBO J 27: 2557–2566.
44. Cobb NJ, Surewicz WK (2009) Prion diseases and their biochemical mechanisms. Biochemistry 48: 2574–2585.
45. Hess B, Kutzner C, van der Spoel D, Lindahl E (2008) GROMACS 4: Algorithms for highly efficient, load-balanced, and scalable molecular simulation. J Chem Theory Comput 4: 435–447.
46. Berendsen H, van der Spoel D, van Drunen R (1995) GROMACS: A message-passing parallel molecular dynamics implementation. Comp Phys Comm 91: 43–56.
47. van der Spoel D, E Lindahl BH, Groenhof G, Mark AE, Berendsen HJC (2005) GROMACS: Fast, exible and free. J Comp Chem 26: 1701–1719.
48. Hornak V, Abel R, Okur A, Strockbine B, Roitberg A, et al. (2006) Comparison of multiple AMBER force fields and development of improved protein backbone parameters. Proteins Struct Funct Bioinf 65: 712–725.
49. Jorgensen W, J C, Maruda J, Impey R, Klein M (1983) Comparison of simple potential functions for simulating liquid water. J Chem Phys 79: 926–935.
50. DePaul AJ, Thompson EJ, Patel SS, Haldeman K, Sorin EJ (2010) Equilibrium conformational dynamics in an RNA tetraloop from massively parallel molecular dynamics. Nucleic Acids Res 38: 4856–4867.
51. Sorin E, Pande V (2005) Exploring the helix-coil transition via all-atom equilibrium ensemble simulations. Biophysical J 88: 2472–2493.
52. Darden T, York D, Pedersen L (1993) Particle mesh Ewald - an n.log(n) method for ewald sums in large systems. J Chem Phys 98: 10089–10092.
53. Berendsen HJC, Postma JPM, DiNola A, Haak JR (1984) Molecular dynamics with coupling to an external bath. J Chem Phys 81: 3684–3690.
54. Nosé S (1984) A molecular dynamics method for simulations in the canonical ensemble. Mol Phys 52: 255–268.
55. Hoover (1985) Canonical dynamics: equilibrium phase-space distributions. Phys Rev A 31: 1695–1697.
56. Parrinello M, Rahman A (1981) Polymorphic transitions in single crystals: A new molecular dynamics method. J Appl Phys 52: 7182–7190.
57. Humphrey W, Dalke A, Schulten K (1996) VMD - Visual Molecular Dynamics. J Mol Graphics 14: 33–38.
58. Frishman D, Argos P (1995) Knowledge-based secondary structure assignment. Proteins 23: 566–579.
59. Warshel A, Russell S, Churg A (1984) Macroscopic models for studies of electrostatic interactions in proteins - limitations and applicability. Proceedings of the National Academy of Sciences of the United States of America-Biological Sciences 81: 4785–4789.
60. Schutz C, Warshel A (2001) What are the dielectric "constants" of proteins and how to validate electrostatic models? Proteins Struct Funct Genet 44: 400–417.
61. Warshel A, Sharma PK, Kato M, Parson WW (2006) Modeling electrostatic effects in proteins. Biochim Biophys Acta 1764: 1647–1676.
62. Roca M, Messer B, Warshel A (2007) Electrostatic contributions to protein stability and folding energy. FEBS Lett 581: 2065–2071.
63. Roberts E, Eargle J,Wright D, Luthey-Schulten Z (2006) Multiseq: unifying sequence and structure data for evolutionary analysis. BMC Bioinformatics 7: 382.
64. Dolinsky T, Nielsen J, McCammon J, Baker N (2004) PDB2PQR: an automated pipeline for the setup, execution, and analysis of Poisson-Boltzmann electrostatics calculations. Nucleic Acids Res 32: W665–W667.
65. Dolinsky T, Czodrowski P, Li H, Nielsen J, Jensen J, et al. (2007) PDB2PQR: Expanding and upgrading automated preparation of biomolecular structures for molecular simulations. Nucleic Acids Res 35: W522–5.